Graefe's Arch Clin Exp Ophthalmol (2000)
238:385–392

CLINICAL INVESTIGATION

Angela Baumgartner
Christoph K. Hitzenberger
Erdem Ergun
Michael Stur
Harald Sattmann
Wolfgang Drexler
Adolf F. Fercher

Resolution-improved dual-beam and standard optical coherence tomography: a comparison

Received: 19 October 1999
Revised: 19 January 2000
Accepted: 3 February 2000

Presented in part at the annual meeting of the Association for Research in Vision and Ophthalmology, May 1998, Fort Lauderdale, Florida

A.Baumgartner · C.K. Hitzenberger (✉)
H. Sattmann · W. Drexler · A.F. Fercher
Institute of Medical Physics,
University of Vienna,
Währinger Strasse 13, A-1090 Vienna,
Austria
e-mail: Christoph.Hitzenberger@univie.ac.at
Tel.: +43–1–427760711
Fax: +43–1–42779607

E. Ergun · M. Stur
Department of Ophthalmology, Vienna
General Hospital, A-1090 Vienna, Austria

Abstract *Background*: The purpose of the study was to demonstrate the improved axial resolution and longitudinal stability of dual-beam optical coherence tomography (OCT) in comparison to conventional OCT setups used in commercially available OCT instruments. *Methods*: The conventional OCT technique is based on an interferometric setup that is rather sensitive to axial eye motions. We have developed a special dual-beam OCT technique which eliminates the influence of axial eye motions. This is achieved by using the anterior corneal surface as the reference surface for the interferometric ranging. To improve the signal quality, the different wavefront curvatures of beams reflected at cornea and retina are matched by a diffractive optical element. To improve the axial resolution, a broadband synthesized light source with an effective bandwidth of 50 nm is used, and the group dispersion of the ocular media is compensated. Tomographic images were recorded in the fovea and the optic nerve head of healthy volunteers. For comparison purposes, approximately the same locations in the same eyes were imaged by a commercially available OCT instrument. *Results*: Compared to the standard OCT technique, the dual-beam OCT images show considerably improved axial resolution. Especially in tomograms recorded at the fovea, dual-beam OCT resolves microstructural details that are not visible in the standard OCT images. Furthermore, the axial stability of dual-beam OCT enables the recording of exact geometrical contours of fundus layers. *Conclusions*: Dual-beam OCT is able to provide structural information on the ocular fundus that is not obtained with standard OCT. The long recording times of our instrument limit the transverse resolution to 100–150 µm at present.

Introduction

Optical coherence tomography (OCT) has been developed since the beginning of the 1990s as a new non-invasive tool for imaging of the human retina with high precision and resolution [15, 17, 23]. For an overview of the technique see refs. [13, 25]. Since a commercial OCT instrument became available for retinal imaging, numerous investigations of different retinal disorders have demonstrated the diagnostic potential of this new technique [5, 9, 24, 27, 29, 30].

The basic technique of OCT is partial (or low) coherence interferometry (PCI), a technique first applied to the biomedical field for measurement of the axial eye length [14, 18]. PCI records optical A-scans of the measured object, plots of back-reflected intensity as a function of depth position. The classical interferometric setup of PCI and OCT has the drawback of being rather sensitive to longitudinal object motions. This limits the repeatability and therefore the precision that is obtained in living objects. Furthermore, it prevents the determination of the exact position and geometric contour of retinal layers with

respect to a fixed reference point of the eye, e.g., the apex of the cornea. We have developed a special dual-beam interferometric setup which overcomes these problems by using the cornea as the reference surface. Several investigations have demonstrated that this technique can record A-scans of different ocular structures with micrometer precision [8, 10, 19]. However, the poor signal-to-noise ratio of this method made OCT imaging of weakly reflecting retinal layers difficult. This problem could be solved by using a diffractive optical technique [26].

The axial resolution of PCI and OCT depends on the spectral bandwidth of the light used. Increasing the bandwidth improves the resolution. The light source that is presently used in most instruments is a superluminescent diode (SLD) emitting in the near infrared, with a bandwidth $\Delta\lambda \cong 20$ nm which corresponds to an axial resolution of ~15 µm. With a Ti:Al_2O_3 laser as a light source, a resolution of ~4 µm was demonstrated in a shallow object [3]. However, if the ranging or imaging is to be performed through a rather deep dispersive object, as in the case of the retina imaged through the transparent ocular media [12], the dispersion-induced signal broadening deteriorates the resolution, if a bandwidth of more than ~25 nm is used [21]. Furthermore, the dispersion can cause multiple signal peak splitting, which can lead to erroneous signal peaks [20]. To overcome these problems, the dispersion of the ocular media has to be compensated [2, 21].

To exploit the advantages of dual-beam PCI for OCT imaging, especially its insensitivity to axial eye motions, we modified our instrument: (1) We improved the signal-to-noise ratio by using a diffractive optical element, and (2) we improved the axial resolution by employing a broadband synthesized light source in combination with a compensation of the dispersive effects of the ocular media. This instrument is an experimental laboratory setup designed primarily for investigation and demonstration of what should be achievable with future OCT systems. It is the purpose of this paper to present the modified instrument, to show first OCT tomograms recorded with the instrument and to compare them with images recorded by a commercially available OCT system. Finally, we discuss the present limitations of our setup.

Methods

The principle of measuring intraocular distances by dual-beam PCI has been described in previous papers in detail [2, 8, 18]. Therefore, only a brief summary, including the improvements to previous instruments, will be presented here.

Figure 1 shows a sketch of our instrument. A broadband light source, consisting of two spectrally displaced SLDs, emits a light beam of high spatial coherence but short coherence length which illuminates an external Michelson interferometer. The interferometer splits the beam into two coaxial components which have a phase difference corresponding to twice the interferometer arm length difference d (the virtual image of mirror 1 is indicated in the other interferometer arm by a dashed outline, i.e., the distance: beam splitter BS – mirror 1 equals the distance BS – dashed mirror outline). This dual-beam illuminates the eye, where each subcomponent is reflected at the various intraocular interfaces. The reflected beams are superimposed on a photodetector. During the measurement, one of the mirrors of the Michelson interferometer is moved while the photodetector records the signal intensity as a function of the mirror position. If the arm length difference of the Michelson interferometer equals (within an uncertainty equal to the coherence length l_c) one of the intraocular distances to be measured, interferometric modulation will occur at the photodetector. The envelope of this signal is recorded as a function of the interferometer arm length difference d with a personal computer. The signal curves recorded in this way are called PCI scans, or optical A-scans, and contain characteristic signal peaks. From the positions of these peaks on the arm length difference axis, the respective optical intraocular distances (IODs) can be determined: optical IOD=d±l_c. For practical purposes (intensity of light reflection) we measure all optical IODs with respect to the anterior corneal surface as the reference surface. To convert an optical IOD into the appropriate geometrical distance, it must be divided by the group refractive index n_g of the respective medium [12, 18].

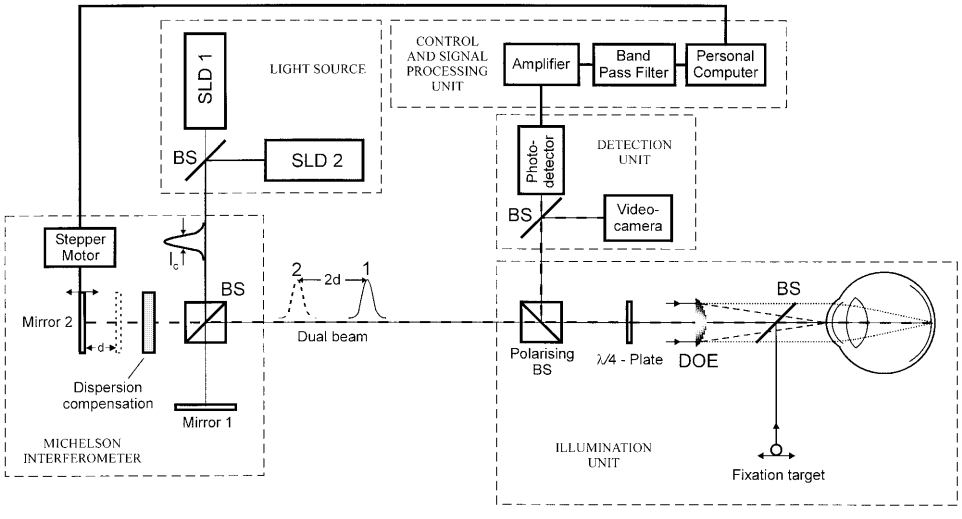

Fig. 1 Sketch of dual-beam OCT instrument (*SLD* superluminescent diode, *BS* beam splitter, *DOE* diffractive optical element)

The major advantage of this dual-beam technique is that it is completely insensitive to axial eye motions, since the reference surface (the cornea) is part of the object, i.e. reference and sampled layers (retina) move simultaneously. Furthermore, the use of the cornea as the reference surface allows one to measure the exact shape of the contours of the retinal layers with respect to the cornea.

The major drawback of our previous dual-beam partial coherence interferometer was the poor signal-to-noise ratio due to the wave-front mismatch of the two interfering beams reflected at the anterior corneal surface and the retina. Since the probing beam is collimated, the light reflected at the retina will be collimated by the optical elements of the human eye (in the case of emmetropic subjects), while the beam reflected at the cornea is divergent. This causes an unfavorable intensity ratio of retinal and corneal beam on the detector and rather narrow interference fringes in the detector plane. Therefore, we had to use a detector with an aperture of only 50 µm diameter in order to ensure that only a single fringe is imaged on the detector surface (which is necessary to obtain a reasonable electric signal from the oscillating interference pattern). In this case, however, the total light power collected by the detector is rather low, causing a poor signal-to-noise ratio. To overcome this drawback we implemented a special diffractive optical element for wave-front matching (see Fig. 1) [2, 26]. This sort of Fresnel's zone lens is located in front of the eye and focuses 40% of the incident light beam on the vertex of the cornea (focal length: 70 mm). The other collimated parallel part of the beam (60%) passes through uninfluenced. This part of the beam will be focused onto the retina (in case of emmetropic subjects) by the optical elements of the human eye. The beams remitted from the anterior corneal surface and the retina will thereby both be converted into parallel beams when passing again through the diffractive optical element on their way back to the detection unit. Since the interference now takes place between two collimated parallel beams, there will be only one (very wide) interference fringe whose light power oscillation will be much stronger than that of the narrow fringes obtained previously. In this way, the signal-to-noise ratio for retinal in vivo signals was improved by about 20–25 dB [2].

The axial resolution of PCI and OCT is approximately equal to the coherence length l_c of the light source used, which is inversely proportional to the source spectral bandwidth $\Delta\lambda$. The usual light source employed in PCI and OCT is an SLD which typically emits at a center wavelength λ_0=830 nm with a bandwidth $\Delta\lambda\cong$25 nm. This corresponds to a (round trip) coherence length $l_c\cong$12 µm [32]. To improve the axial resolution, we used a synthesized light source generated by superimposing two SLDs (EG&G C86142E, EG&G Optoelectronics, Canada) with different center wavelengths (λ_{01}=830 nm, $\Delta\lambda_1$=26 nm, λ_{02}=855 nm, $\Delta\lambda_2$=25 nm). Due to a beat effect [7, 28, 34] these two combined light sources have an effective spectral width of $\Delta\lambda_{eff}$=50 nm. The coherence length of this synthesized light source is $l_c\cong$8 µm [2], corresponding to an axial resolution of ≅6 µm after division by the mean group refractive index 1.354 of the ocular media [12].

If one of the beams in a PCI system travels through a dispersive medium while the other travels through air, the coherence envelope of the optical A-scan broadens and the resolution decreases. This effect increases with increasing source bandwidth, increasing object length, and increasing group dispersion of the object media. Assuming a mean axial eye length of 24 mm, the signal width, after passing through the eye media twice ,to the retina and back, is ~16.2 µm in case of a single SLD with $\Delta\lambda$=26 nm and ~21 µm in case of the combination source with $\Delta\lambda_{eff}$=50 nm [21]. This means that the resolution in the case of larger source bandwidth is not improved, but degraded. In order to obtain the optimum resolution possible with the broadband light source, the group dispersion of the ocular media has to be compensated. This can be achieved by placing a dispersive element in the longer arm of the external Michelson interferometer (see Fig. 1). This element has to fulfill the condition $L_{ce}\cdot GD_{ce}=L_{ob}\cdot GD_{ob}$, where L is the geometric length, GD the group dispersion (defined as derivative of the group index with respect to the wavelength), and the indices ce and ob refer to the compensating element and the object, respectively. As a dispersion-compensating element, we used a plane parallel plate of BK7 optical glass with L_{ce}=12 mm and $GD_{ce}=-3.3\cdot10^{-5}$/nm at a wavelength of λ=840 nm [33]. This element compensates the group dispersion of an eye with axial length of L_{ob}=24 mm and mean $GD\cong-1.83\cdot10^{-5}$/nm (in the wavelength range 815–855 nm [12]) to within a few percent.

For tomographic recordings a separate fixation light was installed in front of the eye under investigation which encloses an adjustable vertical and horizontal angle with the measuring beam and is collimated in order to make the subject look towards infinity. This allows the rotation of the eye to be measured in order to adjust a defined arbitrary angle between vision axis and measuring direction. Once the eye looks at the fixation target, it is aligned with the measuring beam so that the two image points of the anterior corneal surface and the retina are centered and become confocal on the detector. For observation purposes the detection plane is imaged on a CCD camera where the confocal alignment can be monitored.

To obtain OCT images several averaged optical A-scans are recorded at equidistant angles to the vision axis. Each averaged A-scan is the mean of up to eight single A-scans recorded along the same direction (for further improvement of the signal-to-noise ratio). The angle increment was 0.5° corresponding to length increments of ~150 µm on the retina. The intensity values of the averaged optical A-scans are converted into pixel colors (logarithmic scale) and mounted to form a two-dimensional false color image. The pixels between the individual scanning directions are obtained by linear interpolation. For the interpretation of the OCT images recorded in this way, one has to bear in mind that the ordinate shows optical distances (OD) to the cornea. OD is defined as $\sum L_i n_{g,i}$, where L_i is the geometrical length of the i-th individual optical element that has a group index $n_{g,i}$. In the eye, the individual optical elements over which the sum has to be taken are the cornea, aqueous, lens, vitreous, and the several retinal layers. For a perfect conversion of optical to geometrical distance (GD), each individual OD would have to be divided by the respective group index [12] and the resulting geometrical lengths would have to be summed. Since the lengths of the individual elements were not measured in the present work, one can use, to a good approximation, a mean group index $n_{g,m}$=1.354 [12] to convert the optical to the geometrical distance: $GD=OD/n_{g,m}$.

Informed consent was obtained from all subjects in this study after the nature and possible consequences of the study had been explained. The study was approved by the ethics committee of Vienna University School of Medicine.

Tomographic recordings were performed in healthy, volunteer subjects who were emmetropic or moderately myopic (up to –2 diopters). Recordings were taken from the fovea and the optic nerve head. OCT recordings consisted of optical A-scans 3 mm deep. Each single A-scan takes approximately 0.4 s. Performing eight single scans for one averaged A-scan for each measurement direction, the maximum time of continuous illumination of one point on the retina is about 4–5 s. During this time the eye is illuminated with a (spatially) coherent light power of approximately 200 µW or an intensity of 520 µW/cm2 (averaged over a 7 mm aperture). This is permitted for 25 min for a wavelength of λ=830 nm in the case of "intra-beam-viewing" [1]. Since only 60% of the incident light power is focused at the retina (the rest is focused at the cornea), the safety limit is met.

For comparison purposes, we recorded approximately the same areas of the same eyes with a commercial OCT instrument (Humphrey Instruments, San Leandro, Calif.). This instrument is based on a classical interferometric setup, i.e., it is sensitive to axial eye motions. One hundred optical A-scans are recorded in 1 s with this instrument; no averaging of A-scans is performed. The instrument uses a single SLD as a light source; no dispersion compensation is

used. Therefore, an axial resolution of ~16 µm, or ~12 µm after division by the group index of the ocular media, can be expected.

Results

To demonstrate the improvement of axial resolution associated with the increased source bandwidth and dispersion compensation, we recorded two OCT tomograms of the same area of the same human eye in vivo with our dual-beam OCT instrument (see Fig. 2). A horizontal section through the fovea centralis, from 5° temporal to 5° nasal, is shown. This corresponds to a transverse scan width of ~3 mm on the retina. Figure 2a was recorded with a single SLD ($\Delta\lambda$=26 nm) switched on and with the dispersion-compensating element removed. Several microstructural layers can be observed in this figure, the inner limiting membrane (ILM), the foveal depression, the nearly transparent retina, and highly reflective layers at the posterior side of the retina. The uppermost layer is probably the ILM separating the retinal structures from the vitreous. Approximately 390 µm behind the ILM, three different layers can be observed which, however, partly overlap (the color coding on a logarithmic scale tends to reduce the visibility of closely spaced details). In Fig. 2b the synthesized light source with $\Delta\lambda_{eff}$=50 nm is used, i.e., both SLDs are switched on, and the dispersion-compensating element is used. Improved axial resolution can be seen. The three layers posterior to the retina are much better separated and observed as three narrow bands. From individual A-scans a resolution improvement by a factor of ~1.7 was demonstrated [2].

The slight axial shift of the retinal layers between the tomograms of Fig. 2a and Fig. 2b is caused by imperfect recalibration of the instrument after insertion of the dispersion-compensating element (this element increases the optical path length in the corresponding interferometer arm; this was accounted for by calculation, not by an exact mechanical recalibration, which, of course, would be possible). The somewhat weaker signal intensity between the ILM and the triple layer is probably caused by the somewhat poorer signal-to-noise ratio due to imperfect overlapping of the two beams of the synthesized light source.

Figure 3 shows retinal tomograms recorded by dual-beam OCT (Fig. 3a, b) and by the Humphrey OCT (Fig. 3c, d) in the same eye. The images on the left (a, c) show horizontal cross sections of the fovea, those on the right (b, d) show horizontal sections through the optic nerve head. The dual-beam OCT images were recorded with the synthesized light source and with dispersion compensation. Especially in the case of the foveal tomograms (Fig. 3a, c) the improved axial resolution of the dual-beam OCT can be observed. The triple layer at the posterior side of the retina is visible in most parts of the image. This fine structure is not resolved by the Humphrey

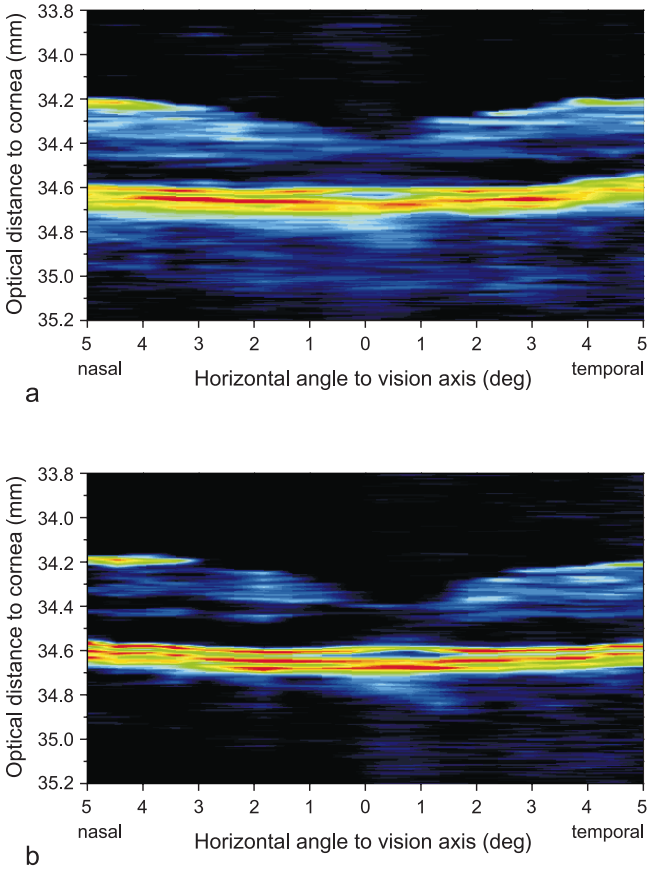

Fig. 2a, b Retinal tomograms recorded by dual-beam OCT in a human eye in vivo, demonstrating different axial resolutions. A horizontal section of the fundus across the fovea from 5° nasal to 5° temporal is shown, corresponding to a width of approximately 3 mm on the retina. The *vertical scale* indicates the optical distance to the anterior corneal surface (to convert it to a geometrical distance, the OD has to be divided by the mean group index $n_{g,m}$=1.354). **a** Single SLD with $\Delta\lambda$=26 nm without dispersion compensation. **b** Synthesized light source of two spectrally displaced SLDs with $\Delta\lambda_{eff}$=50 nm and with dispersion compensation

OCT. Even the separation of the first two layers at the posterior side of the retina is not visible in this image (since the individual A-scans recorded by the Humphrey instrument are not accessible, quantitative comparison of the resolution is not possible). The optic nerve head tomograms look rather similar in overall shape, with somewhat better separation of horizontal layers in the case of the dual-beam OCT image (Fig. 3c). It should be mentioned that the horizontal resolution of the Humphrey OCT is better: the Humphrey tomograms contain 100 A-scans, the dual-beam tomograms contain only 21 (Fig. 3a) and 25 (Fig. 3c) A-scans. However, since there are no fine details in horizontal direction in these images, this advantage is not visible in Fig. 3.

Figure 4 shows retinal tomograms recorded in the same fovea by dual-beam OCT (Fig. 4a; synthesized

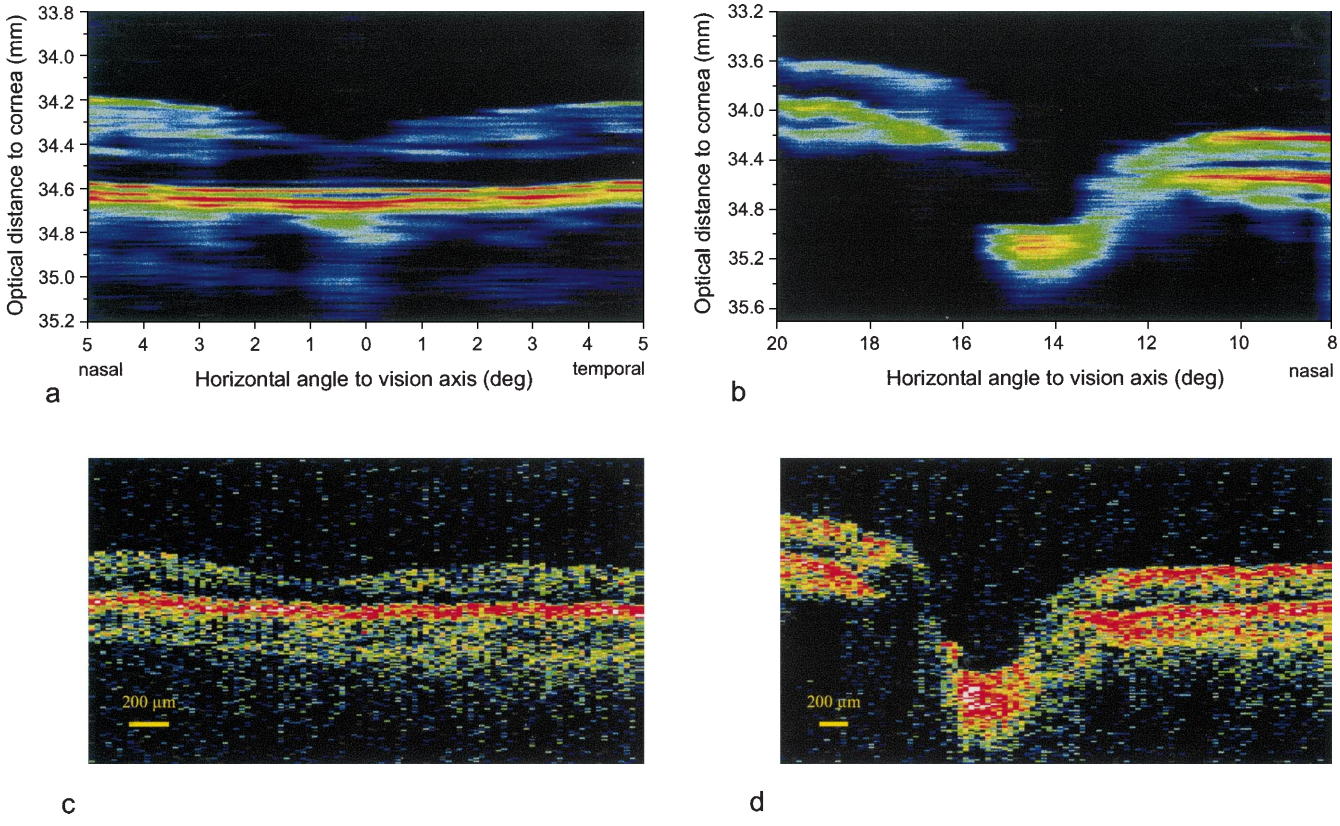

Fig. 3a–d Retinal tomograms recorded by dual-beam OCT (broadband light source and dispersion compensation, optical distance on ordinate) and by the Humphrey OCT in the same human eye in vivo. **a** Fovea recorded by dual-beam OCT. **b** Optic nerve head recorded by dual-beam OCT. **c** Fovea recorded by Humphrey OCT. **d** Optic nerve head recorded by Humphrey OCT

light source, dispersion compensation) and by the Humphrey OCT (Fig. 4b). Again, the improved axial resolution of the dual-beam OCT is observed. Another feature observed in these images is a different geometrical shape of the retina. In the dual-beam OCT image, the retina is inclined from right to left: at 5° temporal, the uppermost of the three layers at the posterior side of the retina is located ≅30.94 mm optical distance behind the anterior corneal surface; at 5° nasal this distance increases to ≅31.10 mm. (The noncontinuous appearance of the layers posterior to the retina is caused by the algorithm interpolating the data points between adjacent A-scans recorded at inclined surfaces.) In a measurement on the next day, these distances were reproducible to within a few micrometers. This result indicates that the dual-beam OCT system is capable of determining the overall geometric shape of the retinal curvature: the optic axis of the eye intersects the retina approximately half-way between the fovea and the optic nerve head; therefore, the distance between cornea and retina should be somewhat larger at the nasal side of the fovea.

The Humphrey OCT image, on the other hand, shows a different shape of the retinal layers: a slight inclination from left to right, with a somewhat wavy appearance superimposed on this slope. This different overall shape of the retina is probably caused by slight object motions during the recording of the Humphrey OCT image which prevent the determination of the exact position of the retinal layers with respect to the cornea.

Discussion

We have demonstrated that dual-beam OCT is capable of providing useful information on the microstructure of the human ocular fundus. Compared to previous OCT images recorded with this technique [9, 15], the signal-to-noise ratio is considerably improved by the wave front matching accomplished with the diffractive optical element. Compared to other wave front matching techniques [4, 31], the diffractive optical element is lightweight, cheap, easier to align, and does not restrict the aperture of the retinal beam, which would increase the beam focus diameter on the retina and therefore might degrade the transverse resolution. From the viewpoint of the signal-to-noise ratio, the dual-beam OCT images are now comparable to those of the Humphrey OCT instrument; however, it should be mentioned that we used signal averaging only with the dual-beam technique.

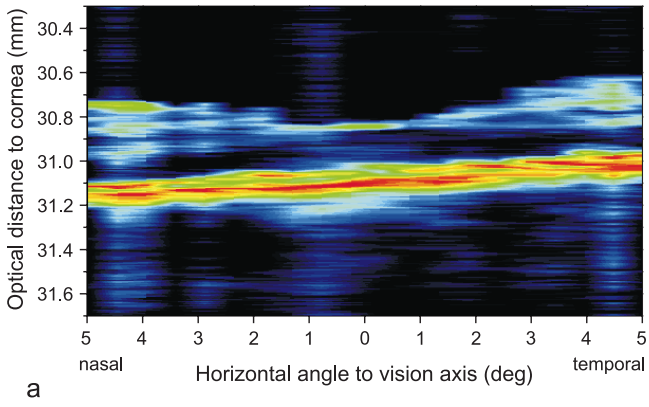

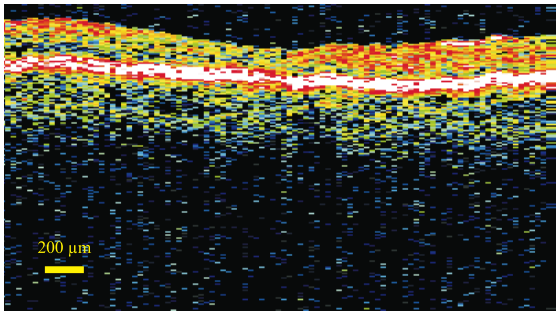

Fig. 4a, b Retinal tomograms recorded by dual-beam OCT (broadband light source and dispersion compensation, optical distance on ordinate) and by the Humphrey OCT in the same human eye in vivo. **a** Fovea recorded by dual-beam OCT; the inclination of the retinal layers indicates the true geometrical contour of the eyeball. **b** Fovea recorded by Humphrey OCT; slight axial eye motions during the recording distort the true geometrical contour of the eyeball

The axial resolution of OCT depends on the source bandwidth and on the dispersion of the object. If only one SLD with $\Delta\lambda \cong 25$ nm is used and the dispersion of the ocular media is not compensated for, an axial resolution of ~12 µm geometrical distance can be expected in the retina. This corresponds to the case of Fig. 2a and to the images recorded with the Humphrey OCT. Systems with higher resolution using broadband Ti:Al_2O_3 sources have so far been used only for ranging and imaging within tissues with a total thickness of a few hundred micrometers [3, 6]. In this case, the dispersive effect of the thin tissue has a negligible effect on the signal width and hence on the resolution. However, if measurements are performed through the relatively thick ocular media to the retina, dispersion becomes important. It has to be compensated for, if a light source with greater bandwidth than that of a single SLD is used. Otherwise, the signal width would increase and hence the resolution be degraded [21]. Furthermore, erroneous signals caused by dispersion-induced signal peak splitting can occur [20].

We have recently demonstrated a signal width of 5 µm (geometrical distance) in an optical A-scan of a human retina in vivo by employing a broadband SLD ($\Delta\lambda$~60 nm) with dispersion compensation [21]. Since the output power of this SLD was lower and the spatial coherence of the source was worse than that of usual SLDs [22], the signal-to-noise ratio was rather poor in that case. Therefore, we preferred to use a synthesized light source with $\lambda_{eff} \cong 50$ nm generated by superimposing two spectrally displaced SLDs in this work. With this light source and dispersion compensation, an axial resolution of ~6 µm geometrical distance in the retina is expected. This corresponds to Fig. 2b. The improved axial resolution, compared to Fig. 2a, is clearly observed.

Compared to the Humphrey OCT, the axial resolution of dual-beam OCT is considerably improved (see Figs. 3, 4). The triplicate band structure observed at the posterior side of the retina in foveal tomograms is not visible in the Humphrey OCT images (see Figs. 2, 3). This is not only due to the larger source bandwidth and dispersion compensation of the dual-beam OCT system. Even the dual-beam OCT images recorded with the single SLD without dispersion compensation show better axial resolution than the Humphrey tomograms (compare Fig. 2a with Figs. 3c, 4b) although light source and dispersion effects should be equal in this case. The reason for the poorer axial resolution of the Humphrey OCT might be its sensitivity to slight axial ocular motions during the measurement, which might “smear out” fine details.

The insensitivity to axial eye motions is another main advantage of our OCT system. The dual-beam OCT images in this work were recorded with an experimental laboratory set-up where each scanning angle had to be adjusted manually. Furthermore, at each scanning angle several A-scans were recorded for signal averaging. Therefore the total scanning time was several minutes. Within this long measurement time, several eye blinks occur. The subject can even take a break, sit back, and rest between the recordings of the individual A-scans making up a tomogram. In spite of this long measuring time and its associated eye movements, the individual A-scans were mounted to the OCT images without any additional digital image processing required to correlate the longitudinal positions of the A-scans. This clearly demonstrates the exceptional axial stability of the dual-beam OCT technique, which might be helpful in cases where digital postprocessing of the images could lead to loss of fine image details.

This insensitivity to axial eye motions enables the exact location of retinal layers with respect to the anterior corneal surface. As a first step, we have demonstrated that our technique is capable of determining the inclination of the retinal layers (Fig. 4). This method can be used to determine the geometrical contour of the eyeball in the imaged area with very high precision. This might

be useful in studies related to ocular growth and development of myopia, where the exact dimensions of the eye ball have to be determined [11]. This is not possible with the Humphrey OCT system.

A drawback of our instrument is the poorer transverse resolution and the long measurement time. Since the measurement takes several minutes, the transverse resolution is limited by microsaccades to an angular resolution of ~1/3° [16]. This corresponds to a transverse distance of ~100 µm on the retina. The Humphrey OCT, on the other hand, records 100 A-scans in 1 s. A typical Humphrey tomogram consists of 100 A-scans over a transverse distance of ~3 mm on the retina. This corresponds to a transverse sampling distance of ~30 µm and is equal to the resolution obtained in the corresponding OCT images (the physical limit of the transverse resolution is determined by the beam focus diameter on the retina, which is ~10 µm). However, the slow speed and, therefore, the poor transverse resolution of our instrument is not a fundamental problem of the dual-beam technique but merely a question of the simple scanning method we used in our laboratory work. By implementing an x-y scanner, the speed of our system could be improved to match that of the Humphrey OCT instrument. In this way, the same transverse resolution should be obtained. However, to achieve this task, some problems with the alignment of the transverse scanning dual-beam remain to be solved.

Acknowledgement Supported by grant P9781-MED from the Austrian Fonds zur Förderung der wissenschaftlichen Forschung.

References

1. American National Standards Institute (1993) Safe use of lasers. ANSI Z 136.1, American National Standards Institute, New York
2. Baumgartner A, Hitzenberger CK, Sattmann H, Drexler W, Fercher AF (1998) Signal and resolution enhancements in dual-beam optical coherence tomography of the human eye. J Biomed Opt 3:45–54
3. Bouma B, Tearney GJ, Boppart SA, Hee MR, Brezinski ME, Fujimoto JG (1995) High-resolution optical coherence tomographic imaging using a mode-locked Ti:Al_2O_3 laser source. Opt Lett 20:1486–1488
4. Chen S, Wang DN, Grattan KTV, Palmer AW, Dick GL (1993) A compact optical device for eye-length measurement. IEEE Photonics Technol Lett 5:729–731
5. Christoffersen N, Sander B, Larsen M (1998) Precipitation of hard exudate after resorption of intraretinal edema after treatment of retinal branch vein occlusion. Am J Ophthalmol 126:454–456
6. Clivaz X, Marquis-Weible F, Salathé RP (1993) 1.5 µm resolution optical low coherence reflectometry in biological tissues. Proc SPIE 2083:338–346
7. Drexler W, Hitzenberger CK, Baumgartner A, Findl O, Sattmann H, Fercher AF (1996) Multiple wavelength partial coherence interferometry. Proc SPIE 2930:194–201
8. Drexler W, Baumgartner A, Findl O, Hitzenberger CK, Sattmann H, Fercher AF (1997) Submicrometer precision biometry of the anterior segment of the human eye. Invest Ophthalmol Vis Sci 38:1304–1313
9. Drexler W, Findl O, Menapace R, Kruger A, Wedrich A, Rainer G, Baumgartner A, Hitzenberger CK, Fercher AF (1998) Dual-beam optical coherence tomography: signal identification for ophthalmologic diagnosis. J Biomed Opt 3:55–65
10. Drexler W, Findl O, Menapace R, Rainer G, Vass C, Hitzenberger CK, Fercher AF (1998) Partial coherence interferometry: a novel approach to biometry in cataract surgery. Am J Ophthalmol 126:524–534
11. Drexler W, Findl O, Schmetterer L, Hitzenberger CK, Fercher AF (1998) Eye elongation during accommodation in humans – differences between emmetropes and myopes. Invest Ophthalmol Vis Sci 39:2140–2147
12. Drexler W, Hitzenberger CK, Baumgartner A, Findl O, Sattmann H, Fercher AF (1998) Investigation of dispersion effects in ocular media by multiple wavelength partial coherence interferometry. Exp Eye Res 66:25–33
13. Fercher AF (1996) Optical coherence tomography. J Biomed Opt 1:157–173
14. Fercher AF, Roth E (1986) Ophthalmic laser interferometry. Proc SPIE 658:48–51
15. Fercher AF, Hitzenberger CK, Drexler W, Kamp G, Sattmann H (1993) In vivo optical coherence tomography. Am J Ophthalmol 116:113–114
16. Hart WM Jr (1987) The temporal responsiveness of vision. In: Moses RA, Hart WM Jr (eds) Adler's physiology of the eye. Mosby, St. Louis, p 436
17. Hee MR, Izatt JA, Swanson EA, Huang D, Schuman JS, Lin CP, Puliafito CA, Fujimoto JG (1995) Optical coherence tomography of the human retina. Arch Ophthalmol 113:325–332
18. Hitzenberger CK (1991) Optical measurement of the axial eye length by laser Doppler interferometry. Invest Ophthalmol Vis Sci 32:616–624
19. Hitzenberger CK, Baumgartner A, Drexler W, Fercher AF (1994) Interferometric measurement of corneal thickness with micrometer precision. Am J Ophthalmol 118:468–476
20. Hitzenberger CK, Baumgartner A, Fercher AF (1998) Dispersion induced multiple signal peak splitting in partial coherence interferometry. Opt Commun 154:179–185
21. Hitzenberger CK, Baumgartner A, Drexler W, Fercher AF (1999) Dispersion effects in partial coherence interferometry: implications for intraocular ranging. J Biomed Opt 4:144–151
22. Hitzenberger CK, Danner M, Drexler W, Fercher AF (1999) Measurement of the spatial coherence of superluminescent diodes. J Mod Optics 46:1763–1774
23. Huang D, Swanson EA, LinCP, Schuman JS, Stinson WG, Chang W, Hee MR, Flotte T, Gregory K, Puliafito CA, Fujimoto JG (1991) Optical coherence tomography. Science 254:1178–1181
24. Krivoy D, Gentile R, Liebmann JM, Stegman Z, Walsh JB, Ritch R (1996) Imaging congenital optic disc pits and associated maculopathy using optical coherence tomography. Arch Ophthalmol 114:165–170

25. Masters BR (1999) Early development of optical low-coherence reflectometry and some recent biomedical applications. J Biomed Opt 4:236–247
26. Möller B, Rudolph G, Klopffleisch A, Donnerhacke KH, Dorsel A (1996) Application of diffractive optics for axial eye length measurement using partial coherence interferometry. Proc SPIE 2930:175–182
27. Puliafito CA, Hee MR, Lin CP, Reichel E, Schuman JS, Duker JS, Izatt JA, Swanson EA, Fujimoto JG (1995) Imaging of macular diseases with optical coherence tomography. Ophthalmology 102:217–229
28. Rao YJ, Ning YN, Jackson DA (1993) Synthesized source for white-light sensing systems. Opt Lett 18:462–464
29. Schaudig U, Hassenstein A, Bernd A, Walter A, Richard G (1998) Limitations of imaging choroidal tumors in vivo by optical coherence tomography. Graefe's Arch Clin Exp Ophthalmol 236:588–592
30. Schuman JS, Hee MR, Puliafito CA, Wong C, Pedut-Kloizman T, Lin CP, Hertzmark E, Izatt JA, Swanson EA, Fujimoto JG (1995) Quantification of nerve fiber layer thickness in normal and glaucomatous eyes using optical coherence tomography. Arch Ophthalmol 113:586–596
31. Sekine A, Minegishi I, Koizumi H (1993) Axial eye-length measurement by wavelength-shift interferometry. J Opt Soc Am A 10:1651–1655
32. Swanson EA, Huang D, Hee MR, Fujimoto JG, Lin CP, Puliafito CA (1992) High-speed optical coherence domain reflectometry. Opt Lett 17:151–153
33. Tropf WJ, Thomas M, Harris TJ (1995) Properties of crystals and glasses. In: Bass M, Van Stryland EW, Williams DR, Wolfe WL (eds) Handbook of optics, 2nd edn, vol II. Mc Graw-Hill, New York, p 33.67
34. Wang DN, Ning YN, Grattan KTV, Palmer AW, Weir K (1994) Optimized multiwavelength combination sources for interferometric use. Appl Opt 33:7326–7333